A Persistent, Large-Scale, and Ordered Electrodynamic Connection Between Saturn and Its Main Rings

A. H. Sulaiman[1] (iD), W. M. Farrell[2] (iD), S.-Y. Ye[1] (iD), W. S. Kurth[1] (iD), D. A. Gurnett[1] (iD), G. B. Hospodarsky[1] (iD), J. D. Menietti[1] (iD), D. Píša[3] (iD), G. J. Hunt[4] (iD), O. Agiwal[4] (iD), and M. K. Dougherty[4] (iD)

[1]Department of Physics and Astronomy, University of Iowa, Iowa City, IA, USA, [2]NASA/Goddard Space Flight Center, Greenbelt, MD, USA, [3]Institute of Atmospheric Physics CAS, Prague, Czech Republic, [4]Blackett Laboratory, Imperial College London, London, UK

Abstract Auroral hiss emissions are ubiquitous in planetary magnetospheres, particularly in regions where electric current systems are present. They are generally diagnostic of electrodynamic coupling between conductive bodies, thus making auroral and moon-connected magnetic field lines prime locations for their detection. However, the role of Saturn's rings as a dynamic conductive body has been elusive and of great interest to the community. Cassini's Grand Finale orbits afforded a unique opportunity to directly sample magnetic field lines connected to the main rings. Here we provide strong evidence for the persistent and organized presence of auroral hiss demonstrably associated with the main rings. This is in contrast to recent observations suggesting that Saturn's rings may be barriers to field-aligned currents. Our results provide a new view of Saturn's rings as a dynamic system that is in continuous and ordered electrodynamic coupling with the planet.

1. Introduction

Saturn's spin-aligned planetary magnetic field merges both the planet's kronographic and magnetic coordinate systems, with a small northward shift of the magnetic equator measured at 0.047 R_S (1 R_S = 60,268 km; Saturn radius) (Dougherty et al., 2018). This means that a magnetic field line intersects an invariant radial distance on the ring plane that is independent of the planet's rotation phase. Ring-connected field lines of a given radial distance have their foot points anchored to a unique pair of magnetic conjugate latitudes, which transforms to an unequal pair of kronographic latitudes by virtue of the northward offset (higher in the northern and lower in the southern hemispheres). Latitudinal variations in properties of Saturn's ionosphere are therefore, to some extent, manifestations of the ring's surface (Connerney, 1986). This one-to-one ionosphere ring mapping has been invoked to explain remotely observed anomalously low electron densities in Saturn's ionosphere as the influx of exogenous water from the ring plane channeling along magnetic field lines and depositing onto their conjugate midlatitudes (Connerney & Waite, 1984; O'Donoghue et al., 2013).

In April 2017, the Cassini spacecraft began a series of 22 highly inclined proximal orbits that took it through the gap between the cloud tops and innermost (D) ring before its destruction by controlled deorbit into Saturn's atmosphere. This type of orbit enabled the spacecraft to traverse magnetic field lines connected to all parts of the main rings (D-A), as well as directly sample Saturn's low-latitude ionosphere (Persoon et al., 2018; Wahlund et al., 2018), thus bringing unprecedented spatial coverage of the Saturnian ring system. In situ measurements directly concerning the main rings have revealed multifaceted ring-planet interactions. These include observations of charged nanodust flowing from the rings into Saturn along magnetic field lines as well as falling into its equatorial atmosphere through collisions with exospheric hydrogen (Hsu et al., 2018; Mitchell et al., 2018). Magnetic field observations identified a strong and variable azimuthal component (B_ϕ) within the gap (Dougherty et al., 2018), indicative of a field-aligned electric current. This phenomenon was attributed to the foot points of magnetic field lines connected to kronographic latitudes having different zonal wind speeds. That said, the observations of such B_ϕ signatures terminating at the inner edge of the D ring led to the suggestion that Saturn's icy rings act as barriers to field-aligned currents flowing on these field lines (Khurana, et al., 2018).

During every orbit, high-resolution data from the Radio and Plasma Wave Science instrument (Gurnett et al., 2004) repeatedly showed emissions, commonly known as auroral hiss, on magnetic field lines connected to the main rings. As the name suggests, they are typically found on high-latitude magnetic field lines connected to the auroral zone (Gurnett, 1966; Santolík & Gurnett, 2003) as well as moon-connected field lines mapped to auroral hot spots (Gurnett et al., 1979; Gurnett et al., 2011; Shprits et al., 2018; Sulaiman, Kurth, Hospodarsky, Averkamp, Ye, et al., 2018). Experimentation also demonstrated the generation of these waves by electron beams ejected from the space shuttle (Gurnett et al., 1986). Surprisingly, measurements during traversals of ring-connected field lines (with conjugate midlatitude foot points) have hinted the presence of such emissions (Sulaiman, Kurth, Hospodarsky, Averkamp, Persoon, et al., 2018), first reported during a single flyby over the main rings during Saturn Orbital Insertion (SOI) in 2004 (Xin et al., 2006). These emissions propagate in the whistler mode and exhibit a characteristic funnel or V-shape in electric field frequency-time spectrograms. Here we show a series of events with the majority found to be organized around the magnetic field line connected to the synchronous point and are therefore likely to be part of a ring-ionosphere current system.

2. Auroral Hiss Theory and Observations

The electric field-measuring component of the Radio and Plasma Wave Science instrument comprised a set of three 10-m antennas in a triaxial arrangement. We present high-resolution electric field power spectra from the Wideband Receiver, which had a frequency upper limit of 10.5 or 75 kHz, depending on the mode. Their spectral resolutions were typically 13.6 and 109 Hz, respectively, both with a typical temporal resolution of 125 ms per spectrum. To distinguish between quasi-electrostatic and electromagnetic waves, we used data from the five-channel Waveform Receiver, which provided coarse electric and magnetic field power spectra up to 2.5 kHz.

Saturn's magnetic field was measured by the fluxgate magnetometer (MAG), from which we used the azimuthal B_ϕ and the magnetic field strength $|\boldsymbol{B}|$ to calculate the electron cyclotron frequency, f_{ce}, both at a temporal resolution of one vector per second. During the Grand Finale, MAG operated in its highest range (Range 3) with dynamic range of $\pm44{,}000$ nT. During SOI, MAG operated in Range 2 with dynamic range of $\pm10{,}000$ nT.

The dispersion relation for waves in a cold collisionless plasma is considered (Stix, 1992). Here, the special case for the electron scale, known as the Appleton-Hartree equation, is given by

$$\left(\frac{ck}{\omega}\right)^2 = 1 - \frac{X(1-X)}{1-X-\frac{1}{2}Y^2\sin^2\theta \pm \left(\left(\frac{1}{2}Y^2\sin^2\theta\right)^2 + (1-X)^2 Y^2\cos^2\theta\right)^{1/2}} \tag{1}$$

$$X = \frac{f_{pe}^2}{f^2} \text{ and } Y = \frac{f_{ce}}{f}$$

where f_{pe} [Hz] $= 8{,}980\sqrt{n_e}$ (cm^{-3}) is the electron plasma frequency and f_{ce} [Hz] $= 28|\boldsymbol{B}|$ (nT) is the electron cyclotron frequency, n_e is the electron number density, $|\boldsymbol{B}|$ is the ambient magnetic field strength, c is the speed of light in a vacuum, k is the wavenumber, $\omega = 2\pi f$ is the angular frequency, θ is the angle between the magnetic field and the wave vector $\hat{\boldsymbol{k}}$. This neglects ion effects because the frequencies are generally sufficiently high that the ions play no role in this wave's propagation.

Auroral hiss emissions are typically produced by quasi-electrostatic whistler mode waves propagating along the resonance cone. The resulting ray path (i.e., group velocity) angle with respect to the magnetic field, ψ_{res}, can be expressed as

$$\cos^2\psi_{\text{res}} \simeq \frac{\left(f_{pe}^2 - f^2\right)\left(f_{ce}^2 - f^2\right)}{f_{pe}^2 f_{ce}^2} \tag{2}$$

It is clear from equation (2) that the whistler mode has a theoretical upper frequency cutoff at either the electron plasma frequency, f_{pe}, or the electron cyclotron frequency, f_{ce}, whichever is lower.

AGU
100
ADVANCING EARTH
AND SPACE SCIENCE

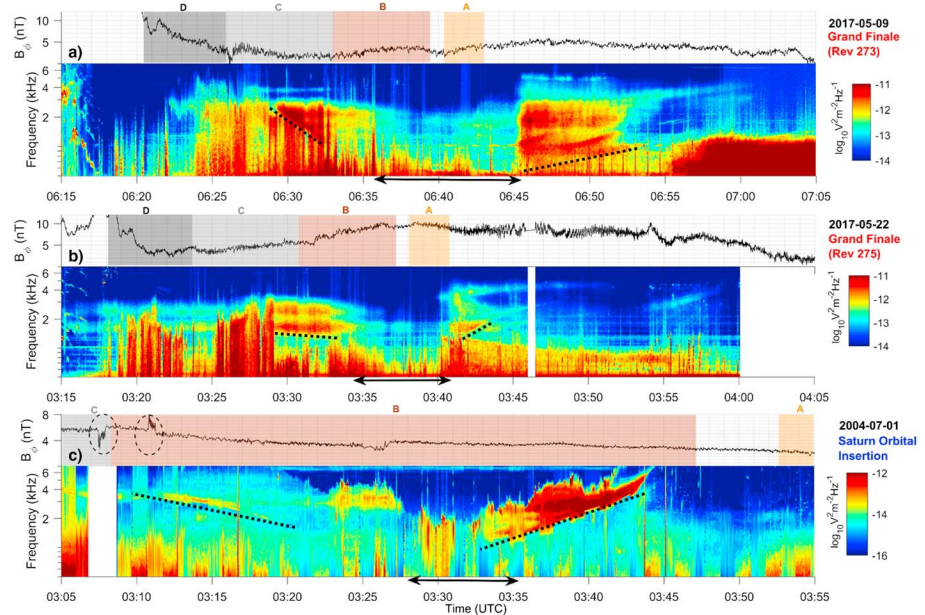**Geophysical Research Letters**

10.1029/2019GL083541

Figure 1. Electric field frequency-time spectrograms of whistler-mode auroral hiss emissions observed on magnetic field lines connected to the main rings (a, b) during the Grand Finale and (c) during Saturn Orbital Insertion. Upper panels are B_ϕ measurements. The shaded time series correspond to times when Cassini traversed L-shells connected to segments of the main rings A, B, C, and D. The double arrows in the horizontal axes highlight the time ranges of the density depletions ("bite outs") which contain the lowest frequencies (or vertices) of each emission, that is, their source magnetic field lines. The black dotted lines are for guidance only and represent the (approximate) V-shapes of the emissions, which are characteristic of auroral hiss. Black dashed ellipses encircling two B_ϕ signatures in (c) are not real and are induced by the acceleration and deceleration of the spacecraft turning.

3. Location and Properties of the Auroral Hiss

Figure 1 presents three time series of auroral hiss emissions when Cassini crossed magnetic field lines connected to the main rings. The upper panels of the observations are the azimuthal component of the magnetic field, B_ϕ (Dougherty et al., 2004), and the lower panels are the electric field frequency-time spectrograms revealing V-shaped whistler mode emissions. Figures 1a and 1b are two of multiple events found during the Grand Finale in the northern and southern hemispheres alike. In comparison, Figure 1c is the single event reported during SOI (Xin et al., 2006). The measured f_{ce} is approximately 500 and 150 kHz during the Grand Finale and SOI, respectively. This makes the upper frequency cutoff of the emissions, of a few kilohertz, coincide with f_{pe}, and hence, a proxy for electron number density, n_e, and the "bite outs" in the upper frequency cutoff (marked by the double-headed arrows) are therefore electron density depletions and these have been linked to density cavities over the rings (Farrell et al., 2018). The absence of power in the magnetic field measuring component of the Waveform Receiver (Figures S1–S3 in the supporting information) confirms the quasi-electrostatic nature of the whistler mode waves associated with the main rings. In this limit ($E/cB \rightarrow \infty$), the waves propagate along the resonance cone. Derived from equation (2), the dispersion relation in this limit in the regime where $f_{ce}^2 \gg f_{pe}^2$ takes the approximation $\sin \psi_{\mathrm{res}} \approx f/f_{pe}$. This leads to higher frequencies propagating at larger ψ_{res} from the source magnetic field line than lower frequencies. The consequence is that the higher frequencies are detected at earlier times as the spacecraft travels toward the source while, conversely, those higher frequencies are detected at later times as the spacecraft travels away from the source. This results in the V-shaped feature seen in frequency-time spectrograms. Since the vertex point of the V-shape represents the lowest frequency, which propagates parallel to the magnetic field, it follows that the time of its detection is coincident with the time of crossing the source magnetic field line.

In the three events, the identification of the vertex points (lowest frequencies), and therefore source magnetic field lines, is obscured by abrupt biteouts due to the existence of electron density depletions over the main rings (Farrell et al., 2018). To mitigate the subjectivity of identifying the source magnetic field line,
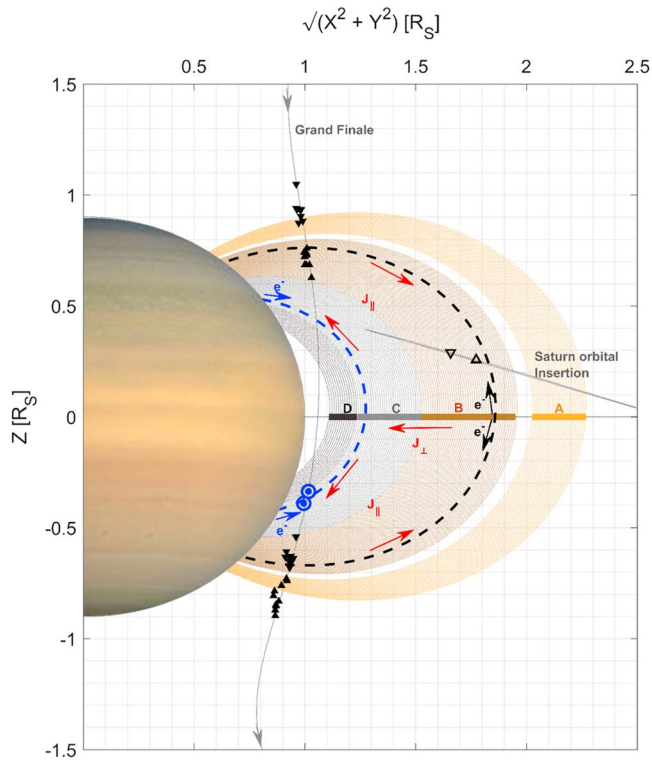
Figure 2. Distribution of observed main ring-connected auroral hiss on ρ-Z space revealing the large-scale system of electrodynamic coupling between Saturn and its rings. Out of the 22 Grand Finale orbits, the signatures were present in all and clearest in 12 of them, used in this plot. The source magnetic field lines are contained within upward pointing (start times) and downward pointing (stop times) triangles: filled triangles during the Grand Finale and open triangles during SOI. These originate from the rings and propagate toward the ionosphere. Blue bull's-eyes are locations of the source magnetic field lines of ring-connected auroral hiss propagating from the ionosphere toward the rings. Since electrons must be codirected with these waves, their expected directions are represented by black arrows along the black dashed magnetic field line, where the theoretical synchronous point is located and by blue arrows along the blue magnetic field line, where the data indicate the antiplanetward auroral hiss are. The field-aligned current system coupling the rings to the ionosphere, as derived from the observations, is represented by red arrows. This picture is consistent with Figure 8 in Xin et al. (2006) proposing the existence of such a current system.

we plot in Figure 2 the ranges within which the source is contained, that is, the extents of the density depletions. Oppositely facing triangles delimit these ranges for the auroral hiss unambiguously identified during the Grand Finale (filled triangles) and the single event identified during SOI (open triangles). With the knowledge that they are quasi-electrostatic and thus propagating along the resonance cone, equation (2) was employed to perform ray tracing analysis and it had been determined that these waves were propagating from the rings, rather than from the ionosphere during both SOI (Xin et al., 2006) and the Grand Finale (Sulaiman, Kurth, Hospodarsky, Averkamp, Persoon, et al., 2018).

The magnetic field observations during the Grand Finale (Figures 1a and 1b) reveal strong B_ϕ deflections in the gap up to the D ring region (Dougherty et al., 2018; Khurana, et al., 2018). The auroral hiss emissions, however, are not coincident with these atmospheric wind-driven electric currents. That said, the combination of a large spacecraft speed and high-inclination orbit resulted in L-shells crossed at a very high rate. This complicates assigning the source magnetic field line of the auroral hiss to a particular segment of the main rings. Fortunately, the near-equatorial orbit and an orbital speed that was ~15 km/s lower during SOI (Figure 1c) meant that the spacecraft spent more time on each ring segment. Here, it is clear that the emission originated from the B ring, as this is where the lowest frequencies of the V-shaped spectral features lie, that is, propagation parallel to the source magnetic field. The difference in the V-shaped spectral features between the Grand Finale and SOI is due to the different angles the spacecraft trajectories cut through the magnetic field lines.

According to the most developed theory, the generation of the whistlermode waves involves the direct coherent amplification via Landau resonance with the parallel component of the electron distribution function (Labelle & Treumann, 2002), that is, $v_\parallel = \omega/k_\parallel$, known as the Cherenkov instability condition. In particular, the quasi-electrostatic mode propagating along the resonance cone (as observed here) has phase speeds much less than the speed of light and would therefore require nonrelativistic electrons for their generation. This interaction has both waves and particles traveling in the same direction (Gurnett et al., 1983). For this reason, auroral hiss is commonly observed in the presence of field-aligned currents (Gurnett et al., 2011; Sulaiman, Kurth, Hospodarsky, Averkamp, Ye, et al., 2018), that is, gradients in B_ϕ. However, a correspondence between the magnetic field and plasma wave data in this study appears equivocal. As shown in Figures 1a and 1b, the B_ϕ component exhibits variability over the main rings, as well as digitization noise from the MAG.

Figure 3 illustrates the set of solutions in velocity space for which the whistler mode can exist, given properties that are descriptive of the Grand Finale events. Since $ck/\omega = c/v_{\mathrm{ph}}$, where v_{ph} is the phase speed, the reciprocal of equation (1) is used to plot solutions of the dispersion relation in phase velocity space, as illustrated in Figure 3. The solutions can be classified into two parts: (i) points that lie on the quasi-electrostatic limit (low $v_{\mathrm{ph}\parallel}/c$) and (ii) points that depart from this limit are in the electromagnetic branch (high $v_{\mathrm{ph}\parallel}/c$). The confirmed quasi-electrostatic nature of these waves implies that they must be generated by low-energy electrons, no different from those generating identical waves on auroral and moon-connected field lines (Gurnett et al., 1979; Gurnett et al., 2011), the latter reported up to 50 eV near Enceladus. Since the Cassini Plasma Spectrometer (CAPS-ELS) was not in operation during the Grand Finale, measurements of electrons in the energy range from 0.6 eV to 28 keV were not available (Young et al., 2004). Fortunately, CAPS-ELS measurements during SOI showed an intense population
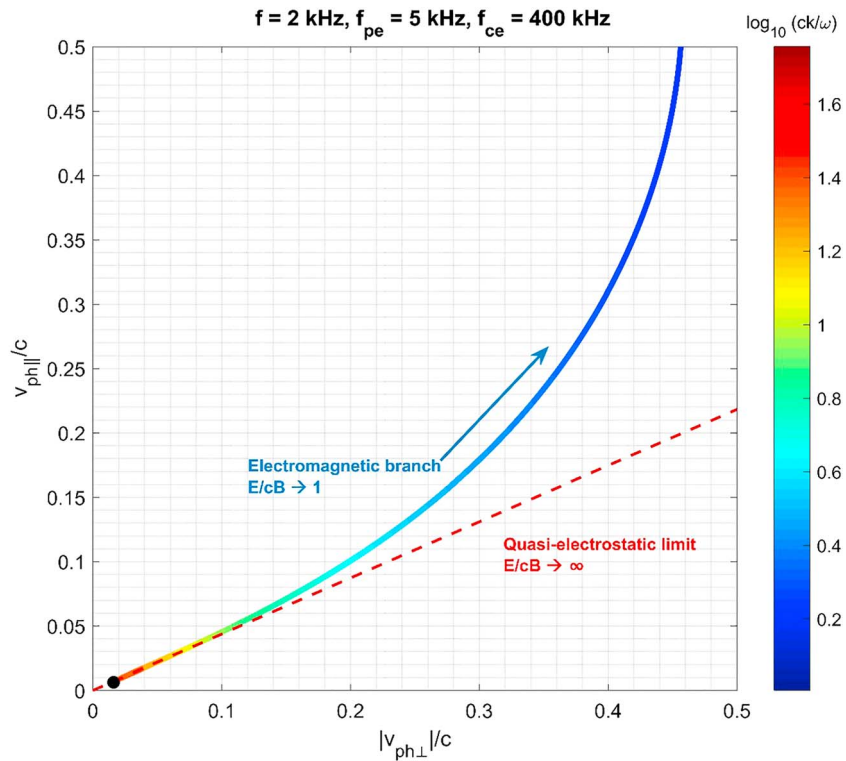
Figure 3. Solutions to the whistler-mode dispersion relation on velocity space color coded by their corresponding index of refraction, ck/ω. These solutions are specific to frequencies observed during the Grand Finale. Waves with indices of refraction much greater than unity become quasi-electrostatic. This mode is generated by very low electron energies. For 10 eV electrons, the Landau resonance condition will amplify waves of $v_{ph\parallel}/c = 0.0063$. The black dot is where this condition intersects the solution—well within the quasi-electrostatic limit. This is confirmed by the lack of magnetic field power in the five-channel waveform receiver, that is, $E/cB \rightarrow \infty$.

of low-energy electrons up to 10 eV over the B ring at ~03:28 UT (Coates et al., 2005), the time when the instrument was switched on. This is right within the range that contains the source magnetic field line in Figure 1c.

The Landau resonance condition requires $v_{\parallel}/c = v_{ph\parallel}/c$, where $v_{\parallel}$ is the parallel electron velocity, for waves to exploit the "free energy" provided by the electrons to grow (Tsurutani & Lakhina, 1997). Taking 10 eV as the upper limit of the electron energy range, assumed to be along the magnetic field line, would yield $v_{\parallel}/c = 0.0063$. The equivalent $v_{ph\parallel}/c$ in Figure 3 intersects a solution well within the quasi-electrostatic range (black dot) and therefore in excellent agreement with the observations. The lack of a correspondence between a gradient in B_{ϕ} and the vertex points of the auroral hiss is likely due to the following combination of factors: (i) assuming that electrons are the primary charge carriers, the field-aligned current desnity, $j_{\parallel} \approx -en_e v_{\parallel}$, where e is the electron charge, $v_{\parallel}$, as shown here, is very low for quasi-electrostatic whistler mode waves, and n_e over (but not in) the B ring is ~0.2 cm^{-3} orders of magnitude lower than measured in the ionosphere (Coates et al., 2005; Persoon et al., 2018), yielding a very weak field-aligned current density, (ii) the presence of magnetic field variability over the main rings, and (iii) digitization noise and the MAG operating at a high range (low sensitivity). Altogether, it is very plausible that these can mask a weak field-aligned current associated with the auroral hiss. While the MAG data are inconclusive for unique signatures of the associated currents, there are possible 1- to 3-nT perturbations present. These ambiguous B_{ϕ} signatures do, however, imply that the associated current density is less than 1 nA/m^2. For example, a field perturbation of ~5 nT over 5° of magnetically mapped colatitude would correspond to a current density of ~1.5 nA/m^2. As we do not observe field perturbations of this magnitude, we conclude the upper limit of the current density to be 1 nA/m^2. In addition, the azimuthal magnetic field could be influenced by other sources as shown by the fits performed by Provan et al. (2019). Indeed, Hunt et al. (2018) showed the presence of the planetary period oscillations in

the azimuthal field component during the closest approach of the ring-grazing orbits prior to the Grand Finale. Finally, it is worth noting that whereas the presence of auroral hiss indicates electron beams associated with a distinct current system, perturbations in B_ϕ are a net effect. This makes it very plausible for B_ϕ perturbations and auroral hiss to decouple.

4. The Ring-Ionosphere Current System

The overall picture in Figure 2 is consistent with the hypothesis put forth by Xin et al. (2006) during SOI. Consider the motions of ring particles and plasma in Keplerian and corotational speeds, respectively. In the rest frame of the rings, a differential speed, $\Delta V = V_{\text{plasma}} - V_{\text{ring}}$, sets up a motional electric field, E' $= -\Delta V \times B$, that drives radial currents, by the action of ring-plasma collisions, across the rings. This would be possible if the collision frequency is sufficiently large to produce a finite transverse conductivity. The synchronous point at ~1.86 R_S is where the two speeds are exactly matched and would therefore represent a dividing point in the radial currents. Inward of the synchronous point, where $V_{\text{ring}} > V_{\text{plasma}}$ (i.e., keplerian speed is greater than corotational speed), the electric field is set up in a direction such that the radial currents travel planetward. Conversely, outside the synchronous point where $V_{\text{plasma}} > V_{\text{ring}}$, the radial currents travel antiplanetward. To conserve charge, field-aligned currents must be directed along $L = 1.86$ toward the synchronous point, that is, electrons symmetrically traveling away from the rings in both hemispheres. The radial currents travelling planetward (antiplanetward) of the synchronous point will terminate at a lower (higher) radial distance and connect to field-aligned currents that close in the lower- (higher-) latitude ionosphere directed away from the rings, that is, electrons travelling from the ionosphere. Presumably, the radial currents will terminate in regions of the rings where ring-plasma collisions are not efficient enough to sustain the net guiding center shift of plasmas in the presence of the motional radial electric field to maintain the radial currents.

Figure 2 shows the auroral hiss observations organized near the L-shell that maps to the synchronous point. Indeed, in both hemispheres, they are launched by electrons traveling away from the rings. The return segment of this current system is likely identified through the observations of auroral hiss and (therefore electrons) traveling from the ionosphere (blue bull's-eye) at a lower radial distance (Sulaiman, Kurth, Hospodarsky, Averkamp, Persoon, et al., 2018). These are analogous to low-altitude observations on Earth's auroral field lines showing whistler-mode emissions generated by upgoing cold ionospheric electrons (James, 1976). Cassini made many fewer observations of these (blue bull's-eye), compared to the auroral hiss linked to around the synchronous point (triangles), since the spacecraft was very close to the source (<1,000 km), and their short observation times (seconds) mean that they can easily be missed. We note that while the auroral hiss observations show clear organization, they do not line up perfectly with the L-shell connecting the theoretical synchronous point at $L \sim 1.86$, possibly due to the plasma not exactly corotating. Xin et al. (2006) constrained the source magnetic field line just planetward of the synchronous point at $L \sim 1.76$. Farrell et al. (2018) showed the spatial extent of the ring density depletions (within which the sources are located) and their distribution in L-shells, clearly distributed around the synchronous point (their Figure 4). Furthermore, there are no clear auroral hiss observations pertaining to the ring-ionosphere current system antiplanetward of the synchronous point. This may be due a current system not existing in that region, perhaps due to the rings becoming more tenuous and therefore not as collisional.

It is interesting to explore the possibility of angular momentum transfer between the rings and Saturn, analogous to auroral and moon current systems. Considering Figure 2 (and the hypothesis by Xin et al., 2006) from a force balance perspective, the effective drag between the ring particles and plasma would be balanced by a $\mathbf{J} \times \mathbf{B}$ force, with $\mathbf{J}$ directed radially across the rings, as laid out earlier, and eventually closing in the ionosphere along field-aligned currents. Regardless of a generation mechanism, we have shown clear evidence of persistent whistler-mode auroral hiss emissions that are demonstrably on magnetic field lines connected to the main rings, and this has been exclusively afforded by the unique coverage of the Grand Finale orbits. These are known to be diagnostics of electrodynamic coupling between conductive bodies, as have been reported on auroral and moon-connected field lines alike. Their observations both originating from the rings (at higher L-shells) and the ionosphere (at lower L-shells) strongly suggest that these are parts of a current system and therefore must be continuous radially across the rings. This makes their spatial

distribution consistent with a large-scale and ordered weak current system between Saturn's main rings and its ionosphere.

References

Coates, A. J., McAndrews, H. J., Rymer, A. M., Young, D. T., Crary, F. J., Maurice, S., et al. (2005). Plasma electrons above Saturn's main rings: CAPS observations. *Geophysical Research Letters*, *32*, L14S09. https://doi.org/10.1029/2005GL022694

Connerney, J. E. P. (1986). Magnetic connection for Saturn's rings and atmosphere. *Geophysical Research Letters*, *13*(8), 773–776. https://doi.org/10.1029/GL013i008p00773

Connerney, J. E. P., & Waite, J. H. (1984). New model of Saturn's ionosphere with an influx of water from the rings. *Nature*, *312*(5990), 136–138. https://doi.org/10.1038/312136a0

Dougherty, M. K., Cao, H., Khurana, K. K., Hunt, G. J., Provan, G., Kellock, S., et al. (2018). Saturn's magnetic field revealed by the Cassini Grand Finale. *Science*, *362*(6410), eaat5434. https://doi.org/10.1126/science.aat5434

Dougherty, M. K., Kellock, S., Southwood, D. J., Balogh, A., Smith, E. J., Tsurutani, B. T., et al. (2004). The Cassini magnetic field investigation. *Space Science Reviews*, *114*(1-4), 331–383. https://doi.org/10.1007/s11214-004-1432-2

Farrell, W. M., Hadid, L. Z., Morooka, M. W., Kurth, W. S., Wahlund, J. E., MacDowall, R. J., et al. (2018). Saturn's plasma density depletions along magnetic field lines connected to the main rings. *Geophysical Research Letters*, *45*, 8104–8110. https://doi.org/10.1029/2018GL078137

Gurnett, D. A. (1966). A satellite study of VLF hiss. *Journal of Geophysical Research*, *71*(23), 5599–5615. https://doi.org/10.1029/JZ071i023p05599

Gurnett, D. A., Averkamp, T. F., Schippers, P., Persoon, A. M., Hospodarsky, G. B., Leisner, J. S., et al. (2004). The Cassini radio and plasma wave investigation. *Space Science Reviews*, *38*(6), 395. https://doi.org/10.1029/2011GL046854

Gurnett, D. A., Averkamp, T. F., Schippers, P., Persoon, A. M., Hospodarsky, G. B., Leisner, J. S., et al. (2011). Auroral hiss, electron beams and standing Alfvén wave currents near Saturn's moon Enceladus. *Geophysical Research Letters*, *38*, L06105. https://doi.org/10.1029/2011GL046854

Gurnett, D. A., Kurth, W. S., & Scarf, F. L. (1979). Auroral hiss observed near the Io plasma torus. *Nature*, *280*(5725), 767–770. https://doi.org/10.1038/280767a0

Gurnett, D. A., Kurth, W. S., Steinberg, J. T., Banks, P. M., Bush, R. I., & Raitt, W. J. (1986). Whistler-mode radiation from the Spacelab 2 electron beam. *Geophysical Research Letters*, *13*(3), 225–228. https://doi.org/10.1029/GL013i003p00225

Gurnett, D. A., Shawhan, S. D., & Shaw, R. R. (1983). Auroral hiss, Z mode radiation, and auroral kilometric radiation in the polar magnetosphere: DE 1 observations. *Journal of Geophysical Research*, *88*(A1), 329. https://doi.org/10.1029/JA088iA01p00329

Hsu, H.-W., Schmidt, J., Kempf, S., Postberg, F., Moragas-Klostermeyer, G., Seiß, M., et al. (2018). In situ collection of dust grains falling from Saturn's rings into its atmosphere. *Science*, *362*(6410), eaat3185. https://doi.org/10.1126/science.aat3185

Hunt, G. J., Provan, G., Cowley, S. W. H., Dougherty, M. K., & Southwood, D. J. (2018). Saturn's planetary period oscillations during the closest approach of Cassini's ring-grazing orbits. *Geophysical Research Letters*, *45*, 4692–4700. https://doi.org/10.1029/2018GL077925

James, H. G. (1976). VLF saucers. *Journal of Geophysical Research*, *81*(4), 501–514. https://doi.org/10.1029/JA081i004p00501

Khurana, K. K., Dougherty, M. K., Provan, G., Hunt, G. J., Kivelson, M. G., Cowley, S. W. H., et al. (2018). Discovery of atmospheric-wind-driven electric currents in Saturn's magnetosphere in the gap between Saturn and its rings. *Geophysical Research Letters*, *45*, 10,068–10,074. https://doi.org/10.1029/2018GL078256

Labelle, J., & Treumann, R. A. (2002). Auroral radio emissions, 1. Hisses, roars, and bursts. *Space Science Reviews*, *101*(3/4), 295–440. https://doi.org/10.1023/A:1020850022070

Mitchell, D. G., Perry, M. E., Hamilton, D. C., Westlake, J. H., Kollmann, P., Smith, H. T., et al. (2018). Dust grains fall from Saturn's D-ring into its equatorial upper atmosphere. *Science*, *362*(6410), eaat2236. https://doi.org/10.1126/science.aat2236

O'Donoghue, J., Stallard, T. S., Melin, H., Jones, G. H., Cowley, S. W. H., Miller, S., et al. (2013). The domination of Saturn's low-latitude ionosphere by ring 'rain'. *Nature*, *496*(7444), 193–195. https://doi.org/10.1038/nature12049

Persoon, A. M., Kurth, W. S., Gurnett, D. A., Groene, J. B., Sulaiman, A. H., Wahlund, J. E., et al. (2018). Electron density distributions in Saturn's ionosphere. *Geophysical Research Letters*, *46*, 3061–3068. https://doi.org/10.1029/2018GL078020

Provan, G., Cowley, S. W. H., Bunce, E. J., Bradley, T. J., Hunt, G. J., Cao, H., & Dougherty, M. K. (2019). Variability of intra-D ring azimuthal magnetic field profiles observed on Cassini's proximal periapsis passes. *Journal of Geophysical Research: Space Physics*, *124*, 379–404. https://doi.org/10.1029/2018JA026121

Santolík, O., & Gurnett, D. A. (2003). Propagation of auroral hiss at high latitudes. *Geophysical Research Letters*, *29*(10), 1481. https://doi.org/10.1029/2001GL013666

Shprits, Y. Y., Menietti, J. D., Drozdov, A. Y., Horne, R. B., Woodfield, E. E., Groene, J. B., et al. (2018). Strong whistler mode waves observed in the vicinity of Jupiter's moons. *Nature Communications*, *9*, 3131. https://doi.org/10.1038/s41467-018-05431-x

Stix, T. H. (1992). *Waves in plasmas*. New York: American Institute of Physics.

Sulaiman, A. H., Kurth, W. S., Hospodarsky, G. B., Averkamp, T. F., Persoon, A. M., Menietti, J. D., et al. (2018). Auroral hiss emissions during Cassini's Grand Finale: Diverse electrodynamic interactions between Saturn and its rings. *Geophysical Research Letters*, *45*, 6782–6789. https://doi.org/10.1029/2018GL077875

Sulaiman, A. H., Kurth, W. S., Hospodarsky, G. B., Averkamp, T. F., Ye, S. Y., Menietti, J. D., et al. (2018). Enceladus auroral hiss emissions during Cassini's Grand Finale. *Geophysical Research Letters*, *45*, 7347–7353. https://doi.org/10.1029/2018GL078130

Tsurutani, B. T., & Lakhina, B. S. (1997). Some basic concepts of wave-particle interactions in collisionless plasmas. *Reviews of Geophysics*, *35*(4), 491–501. https://doi.org/10.1029/97RG02200

Wahlund, J.-E., Morooka, M. W., Hadid, L. Z., Persoon, A. M., Farrell, W. M., Gurnett, D. A., et al. (2018). In situ measurements of Saturn's ionosphere show that it is dynamic and interacts with the rings. *Science*, *359*(6371), 66–68. https://doi.org/10.1126/science.aao4134

Xin, L., Gurnett, D. A., Santolík, O., Kurth, W. S., & Hospodarsky, G. B. (2006). Whistler-mode auroral hiss emissions observed near Saturn's B-ring. *Journal of Geophysical Research*, *111*, A06214. https://doi.org/10.1029/2005JA011432

Young, D. T., Berthelier, J. J., Blanc, M., Burch, J. L., Coates, A. J., Goldstein, R., et al. (2004). Cassini plasma spectrometer investigation. *Space Science Reviews*, *114*(1-4), 1–112. https://doi.org/10.1007/s11214-004-1406-4

Erratum

In the originally published version of this article, there were errors in equation (1). Additionally, in section 3 and in the legend of Figure 3, (E/cB ∞) should have been published as (E/cB $\rightarrow \infty$). These errors have since been corrected, and the present version may be considered the authoritative version of record.